

To appear in the *International Journal of Computational Fluid Dynamics*  
Vol. 00, No. 00, 00 Month 20XX, 1–18

## Near-wall damping in model predictions of separated flows

Martin Skote<sup>a\*</sup> and Stefan Wallin<sup>b</sup>

<sup>a</sup>*School of Mechanical & Aerospace Engineering, Nanyang Technological University, 50 Nanyang Avenue, Singapore 639798;* <sup>b</sup>*Linné FLOW Centre, Department of Mechanics, KTH, SE-100 44 Stockholm, Sweden*

(v4.1 released January 2014)

Different near-wall scalings are reviewed by the use of data from direct numerical simulations (DNS) of attached and separated adverse pressure gradient turbulent boundary layers. The turbulent boundary layer equation is analyzed in order to extend the validity of existing wall damping functions to turbulent boundary layers under severe adverse pressure gradients. A proposed near-wall scaling (Wallin and Johansson 2000) is based on local quantities and the wall distance, which makes it applicable for general CFD methods. It was found to have a similar behaviour as the pressure-gradient corrected analytical  $y^+$  scaling and avoids the inconsistencies present in the  $y^+$  scaling. The performance of the model is illustrated by model computations using explicit algebraic Reynolds stress models with near-wall damping based on different scalings.

**Keywords:** turbulent boundary layer; adverse pressure gradient; separation; turbulence modelling; direct numerical simulation; damping function

### 1. Introduction

Separation continues to be one of the most difficult flow phenomena to predict, both for laminar and turbulent flows. Because of its importance for the efficiency of both aerofoils and turbomachinery a lot of effort has been put into investigations of separating flows, see e.g. Cuvier et al. (2014) for a comprehensive list of references. Although laminar flow is prevalent in many applications, e.g. biochemistry (Mårtensson et al. 2006), biology (Chen and Skote 2015) or even flow control (Ibrahim and Skote 2012), turbulence in an ubiquitous phenomena in vehicle engineering applications due to the transition from laminar to turbulent flow. In addition, turbulent boundary layers around vehicles undergo another major metamorphosis from attached to separated, often caused by geometry of the vehicle. Since the geometry parameters vary widely from case to case, a more general condition of an applied adverse pressure gradient (APG) is often used to serve as a generalization for the geometry-induced separation.

Two of the most widely used turbulence models, the  $K - \omega$  model, Wilcox (1994), and the  $K - \omega$  SST model, Menter (1994), have gained popularity due to their applicability to weakly separated flows around slender bodies (such as aerofoils). Also the one-equation Spalart-Allmaras model by Spalart and Allmaras (1994) was developed precisely for these kind of geometries. However, these models perform less well for bluff bodies. In addition, the above described models, whether they are based on one or two equations, are employing the eddy viscosity concept.

On the other hand, the Hanjalić Reynolds Stress transport (RST) model by Hanjalić, Jakirlić, and Hadžić (1995) utilizes the full transport equations for the Reynolds stresses and thus bypasses the need for eddy viscosity. This model can predict the asymptotic behaviour for high Reynolds numbers as shown by Skote, Henningson, and Henkes (1998). However, numerical stability and

---

\*Corresponding author. Email: mskote@ntu.edu.sg

high computational cost remain severe drawbacks of the model for engineering applications. By simplifying the full transport equations, an explicit algebraic model can be developed (Wallin and Johansson 2000), which mitigates the difficulties associated with the RST model while retaining the advantage of not relying on the eddy viscosity concept.

The aim with this work is to investigate how predictions of turbulent boundary layer flow is affected by the complication of a severe APG and separation. In the near-wall part of the flow, turbulence models often utilize damping functions. Their purpose is to damp various physical quantities in the neighborhood of a wall. One important step towards better model predictions in APG flows is the refinement of the damping functions. A relevant velocity scale is crucial for the correct behaviour of wall damping functions used in turbulence models. For a zero pressure gradient (ZPG) boundary layer, the damping functions and boundary conditions in the logarithmic layer are based on a theory in which the friction velocity,

$$u_\tau \equiv \sqrt{\nu \left. \frac{\partial u}{\partial y} \right|_{y=0}}, \quad (1)$$

is used as a velocity scale. However, in the case of a boundary layer under an APG,  $u_\tau$  is not the relevant velocity scale, especially not for a strong APG and low Reynolds number. In the case of separation this is clear since  $u_\tau$  becomes zero. Wall damping functions based on  $y^+ \equiv y u_\tau / \nu$  are, thus, not appropriate. Other possibilities than  $y^+$  that are used in near-wall damping functions are  $Re_y \equiv \sqrt{K} y / \nu$  or the turbulent Reynolds number  $Re_t \equiv K^2 / \nu \varepsilon$  (see e.g. Wilcox (1993)). These alternatives do not have the singularity caused by that  $u_\tau$  becomes zero. Note that alternatives to the friction velocity as velocity scale naturally enter in the equation governing the inner part of the turbulent boundary layer under any situation where the wall shear stress is affected by outer influences, such as in drag reduced flows, see Skote (2014).

The scaling laws developed in many previous studies have been in a form not suitable for turbulence models. Instead, the aim for the scaling of the velocity profile has often been to create a tool for different prediction methods based on the simplified turbulent boundary-layer equations (TBLE). Many of the earlier theoretical analyses were not performed with the same objectives as we have today. Hence, the results, though interesting in many aspects, perhaps lack a natural potential for direct application to the final goal — to calculate and predict a turbulent boundary layer flow. The motivation for the thorough scaling analysis performed here is that the turbulence modelling can be improved if the correct scaling is used. However, the scalings are entirely motivated by the TBLE itself, i.e. turbulence modelling is disregarded when performing the scaling analysis of the TBLE.

The purpose of the present paper is to utilize direct numerical simulation (DNS) data to develop the near-wall scalings aimed at improving the wall damping functions utilized by the turbulence model. Two turbulent boundary layers subject to adverse pressure gradients (APG) were investigated through DNS by Skote and Henningson (2002). The two APG distributions are quite similar, but the influence of the APG on the flow is strong, creating two very different boundary layer flows. One is everywhere attached (APG1), and the other is separated for a long streamwise section (SEP).

The particular model studied is the fully self-consistent explicit algebraic Reynolds stress model (EARSIM) developed by Wallin and Johansson (2000), which can, in contrast to standard eddy-viscosity two-equation models, be successfully damped in the vicinity of a wall in zero pressure-gradient boundary layers by employing the standard van Driest damping function.

The new velocity scale introduced in section 2.1 is used in the wall damping of the EARSIM model (described in sections 2.2 and 2.3) in section 3. A priori tests with DNS data from the APG1 and SEP cases are presented in sections 3.2 and 3.3, respectively. Comparison with the damping based on  $Re_y$  proposed by Wallin and Johansson (2000) is made in section 3.4, and an example of the performance of EARSIM with the improved damping is given in section 3.5. Conclusions are drawn lastly in section 4.

## 2. Theory

Some basic ideas concerning the velocity scale in the inner part of the turbulent boundary layer under an APG are presented in section 2.1. It is shown that the total shear stress varies linearly in a turbulent boundary layer under a strong APG. The linear behaviour leads to a velocity scale dependent on the normal coordinate, replacing the friction velocity as a velocity scale.

The specific turbulence model (EARSM) used in the present work is described in section 2.2 while the related near-wall corrections are presented in section 2.3.

### 2.1. Scalings in the near-wall region

When neglecting the non-linear, advective terms in the equation describing the streamwise mean flow, i.e. the Reynolds-averaged Navier-Stokes (RANS) equation, the equation governing the inner part of the boundary layer is obtained. This equation can, when using the inner length and velocity scales  $\nu/u_\tau$  and  $u_\tau$  be written,

$$0 = -\frac{\nu}{u_\tau^3} \frac{1}{\rho} \frac{dP}{dx} + \frac{d^2 u^+}{dy^{+2}} - \frac{d}{dy^+} \langle u'v' \rangle^+, \quad (2)$$

where  $\langle u'v' \rangle$  is the Reynolds shear stress. If the term involving the pressure gradient is smaller than the other terms, the equation reduces to the equation governing the inner part of a ZPG boundary layer. However, for strong APG cases at finite Reynolds numbers, this term cannot be neglected. Equation (2) can be integrated to give an expression for the total shear stress,  $\tau^+ \equiv \tau/u_\tau^2$ ,

$$\tau^+ \equiv \frac{du^+}{dy^+} - \langle u'v' \rangle^+ = 1 + \frac{\nu}{u_\tau^3} \frac{1}{\rho} \frac{dP}{dx} y^+. \quad (3)$$

For a zero pressure gradient case, equation (3) predicts a constant shear stress of unity. For an APG case with a freestream distribution of the form  $U \sim x^m$ , the last term in equation (3) can be shown (Skote, Henningson, and Henkes 1998) to decrease with increasing Reynolds number.

When considering a strong APG or separation, A singularity occurs when  $u_\tau$  becomes zero, which can be avoided by introducing the velocity scale,

$$u_p \equiv \left( \nu \frac{1}{\rho} \frac{dP}{dx} \right)^{1/3}. \quad (4)$$

First equation (3) is formulated as

$$\tau^+ = 1 + \left( \frac{u_p}{u_\tau} \right)^3 y^+. \quad (5)$$

The velocity scale  $u_p$  has to be used instead of  $u_\tau$  if the last term in equation (5) becomes very large which happens if  $u_\tau \ll u_p$ , i.e. the boundary layer is close to separation. This was noted by Stratford (1959), Townsend (1961) and Tennekes and Lumley (1972). By multiplying equation (5) by  $(u_\tau/u_p)^2$ , the following expression for  $\tau^p \equiv \tau/u_p^2$  as a function of  $y^p \equiv y u_p/\nu$  is obtained,

$$\tau^p = y^p + \left( \frac{u_\tau}{u_p} \right)^2. \quad (6)$$

Equation (6) has the asymptotic form  $\tau^p = y^p$  when separation is approached. Thus, in this rescaled form, the singularity is avoided.

For the ZPG case, the scaling of the total shear stress with  $u_\tau$  gives a self-similar profile ( $\tau^+ = 1$ ). From equations (5) and (6) it is observed that neither  $u_\tau$  nor  $u_p$  as velocity scale results in a self-similar expression. However, equation (3) can be formulated as

$$\tau^* \equiv \frac{1}{u_*^2} \left( \nu \frac{\partial u}{\partial y} - \langle u'v' \rangle \right) = 1, \quad (7)$$

where  $u_*$  is a velocity scale that depends on  $y$  and can be expressed in either plus or pressure gradient units,

$$u_*^2 = u_\tau^2 + \frac{u_p^3}{u_\tau} y^+ = u_\tau^2 + u_p^2 y^p. \quad (8)$$

Thus, by scaling the total shear stress with  $u_*$ , a self-similar expression is obtained ( $\tau^* = 1$ ). The velocity scale  $u_*$  reduces to  $u_\tau$  if  $u_p$  becomes zero, i.e. for a ZPG boundary layer. If instead  $u_\tau$  becomes zero, i.e. a boundary layer at separation, the velocity scale becomes  $u_* = u_p \sqrt{y^p}$ .

For the special case with  $u_\tau = 0$ , the velocity scale  $u_*$  is zero at the wall. This is natural since the velocity gradient is zero at the wall. Previous investigators of the mixing length theory have also observed the importance of  $u_*$ , see Granville (1989) for references.

From  $u_*$  it is possible to define the length scale  $\nu/u_*$ , and thus a normalized normal coordinate,  $y^* \equiv y u_*/\nu$  which can be written,

$$y^* = \sqrt{(y^+)^2 + (y^p)^3}. \quad (9)$$

If a separated flow is considered, the definition of  $u_\tau$  has to be reconsidered. In the separated region, the wall-normal derivative of the streamwise velocity is negative. Thus, the definition of  $u_\tau$  in equation (1) involves a square root of a negative number. A general definition of  $u_\tau$ , recognizing that  $u_\tau^2$  is directly related to the wall shear stress, is a vector relation  $(u_\tau^2)_i \equiv \nu \partial u_i / \partial y$  and that  $u_\tau = \sqrt{|u_\tau^2|} \geq 0$ . Thus, in order to proceed with the analysis of the equations, the absolute value of the wall shear stress is used in the definition of the friction velocity. Effectively, this means that the definition,

$$u_\tau \equiv \sqrt{-\nu \frac{\partial u}{\partial y} \Big|_{y=0}}, \quad (10)$$

replaces (1).

In the case of a separated flow, the change of direction of the wall shear stress leads to a  $u_*$  as,

$$u_*^2 = -u_\tau^2 + \frac{u_p^3}{u_\tau} y^+ \quad (11)$$

which becomes negative for  $y^+ < (u_\tau/u_p)^3$ , because the shear stress is negative at those values of  $y^+$ . Hence, the length scale  $\nu/u_*$  has to be used with a restriction to positive values of  $u_*^2$ . This leads to a  $y^*$  of the form,

$$y^* = \sqrt{\max\{0, -(y^+)^2 + (y^p)^3\}}. \quad (12)$$

## 2.2. The basic turbulence models

In two-dimensional mean flows, the fully self-consistent explicit algebraic Reynolds stress model may be formulated based on any (quasi-)linear pressure-strain model (see Wallin and Johansson

(2000) and Girimaji (1997) for details). Neglecting the advection and diffusion of the Reynolds stress anisotropy  $a_{ij} \equiv \langle u'_i u'_j \rangle / K - 2\delta_{ij}/3$  results in an implicit and non-linear relation

$$0 = \left( A_3 + A_4 \frac{\mathcal{P}}{\varepsilon} \right) a_{ij} + A_1 S_{ij} - (a_{ik} \Omega_{kj} - \Omega_{ik} a_{kj}) + A_2 \left( a_{ik} S_{kj} + S_{ik} a_{kj} - \frac{2}{3} a_{kl} S_{lk} \delta_{ij} \right), \quad (13)$$

where  $S_{ij} \equiv \tau/2(U_{i,j} + U_{j,i})$  and  $\Omega_{ij} \equiv \tau/2(U_{i,j} - U_{j,i})$  are the symmetric and antisymmetric parts of the velocity gradient tensor normalized by the turbulent time scale  $\tau \equiv K/\varepsilon$ .

In a two-dimensional mean flow the solution for the anisotropy becomes

$$\begin{aligned} a_{12} &= \beta_1 S_{12} + 2\beta_4 S_{11} \Omega_{12} \\ a_{11} &= \beta_1 S_{11} + \beta_2 \left( S_{11}^2 + S_{12}^2 - \frac{1}{3} II_S \right) - 2\beta_4 S_{12} \Omega_{12} \\ a_{22} &= -\beta_1 S_{11} + \beta_2 \left( S_{11}^2 + S_{12}^2 - \frac{1}{3} II_S \right) + 2\beta_4 S_{12} \Omega_{12} \\ a_{33} &= \beta_2 \left( -\frac{1}{3} II_S \right) \end{aligned} \quad (14)$$

where the  $\beta$  coefficients are functions of the flow invariants  $II_S \equiv S_{ij} S_{ji}$  and  $II_\Omega \equiv \Omega_{ij} \Omega_{ji}$  and the model coefficients  $A_{1-4}$  in equation (13). Two different EARSMS will be considered; the "W&J" model, Wallin and Johansson (2000), based on a recalibrated LRR (Launder, Reece, and Rodi 1975) pressure-strain rate model and the "Gir" model, Girimaji (1997), based on the linearized SSG (Speziale, Sarkar, and Gatski 1991) pressure-strain rate model. The corresponding  $A_{1-4}$  coefficients are given in table 1. The "W&J" model results in that the  $\beta_2$  coefficient is zero and as a consequence  $a_{33} = 0$ .

In two-dimensional mean flows the  $\beta$  coefficients are given by

$$\beta_1 = -\frac{A_1 N}{Q}, \beta_2 = 2\frac{A_1 A_2}{Q}, \beta_4 = -\frac{A_1}{Q}, \quad (15)$$

where the denominator is

$$Q = N^2 - 2II_\Omega - \frac{2}{3} A_2^2 II_S. \quad (16)$$

$N$  is given by

$$N = \begin{cases} \frac{A_3}{3} + (P_1 + \sqrt{P_2})^{1/3} + \text{sign}(P_1 - \sqrt{P_2}) |P_1 - \sqrt{P_2}|^{1/3}, & P_2 \geq 0 \\ \frac{A_3}{3} + 2(P_1^2 - P_2)^{1/6} \cos\left(\frac{1}{3} \arccos\left(\frac{P_1}{\sqrt{P_1^2 - P_2}}\right)\right), & P_2 < 0 \end{cases} \quad (17)$$

where

$$\begin{aligned} P_1 &= \left( \frac{A_3^2}{27} + \left( \frac{A_1 A_4}{6} - \frac{2}{9} A_2^2 \right) II_S - \frac{2}{3} II_\Omega \right) A_3 \\ P_2 &= P_1^2 - \left( \frac{A_3^2}{9} + \left( \frac{A_1 A_4}{3} + \frac{2}{9} A_2^2 \right) II_S + \frac{2}{3} II_\Omega \right)^3. \end{aligned} \quad (18)$$

Table 1. The values of the  $A$ -coefficients for different quasi-linear pressure-strain models.

	$A_1$	$A_2$	$A_3$	$A_4$
W&J (Recalibrated LRR)	1.20	0	1.80	2.25
Gir (Linearized SSG)	1.22	0.47	0.88	2.37

### 2.3. Near-wall treatments

In the model proposed by Wallin and Johansson (2000) the correct near-wall behaviour for zero pressure-gradient boundary layers was obtained by modifying the  $\beta$  coefficients using a damping function of the van Driest type. The original form was based on  $y^+$ , but an alternative suggestion of the damping function was based on  $y^T = y^T(Re_y)$  in order of avoiding the singularity in separated flows. The function  $y^T$  was constructed to be similar to  $y^+$  for  $y^+ < 100$  in zero pressure-gradient boundary layers. In this section the different near-wall scalings will be assessed by comparing model predictions using  $y^+$ ,  $y^T$  as well as  $y^*$ .

In a two-dimensional mean flow the near-wall corrections for the "W&J" model reads

$$\begin{aligned}\beta_1 &= f_1 \beta_1^* \\ \beta_2 &= f_1^2 \beta_2^* + (1 - f_1^2) \frac{3B_2 - 4}{\max(\Pi_S, \Pi_S^{eq})} \\ \beta_4 &= f_1^2 \beta_4^* - (1 - f_1^2) \frac{B_2}{2\max(\Pi_S, \Pi_S^{eq})}\end{aligned}\tag{19}$$

where  $\beta_1^*$ ,  $\beta_2^*$  and  $\beta_4^*$  are the "high-Re" uncorrected coefficients given by (15) and the damping function

$$f_1 = 1 - \exp(-y^+/A^+)\tag{20}$$

and the model coefficients

$$\Pi_S^{eq} = 5.74 \quad B_2 = 1.8\tag{21}$$

For the damped expressions the turbulent time scale used for normalizing the velocity gradient tensors must be limited by the viscous scale, such as

$$\tau \equiv \max\left(\frac{K}{\varepsilon}, C_\tau \sqrt{\frac{\nu}{\varepsilon}}\right)\tag{22}$$

where  $C_\tau = 6.0$  is used.

## 3. Evaluation of turbulence models

The results regarding the near-wall flow reported from the well resolved DNS in Skote and Henningson (2002) can be utilized in turbulence model predictions directly as, so called, wall-function boundary conditions. Here we are instead interested in resolving the turbulent boundary layer all the way to the wall and thus the wall damping functions become important.

A short description of the DNS and the turbulent boundary layer flows is given in section 3.1. A priori tests done with DNS data from both simulations are presented in sections 3.2 and 3.3, respectively, together with the development of damping functions. The relation between two length

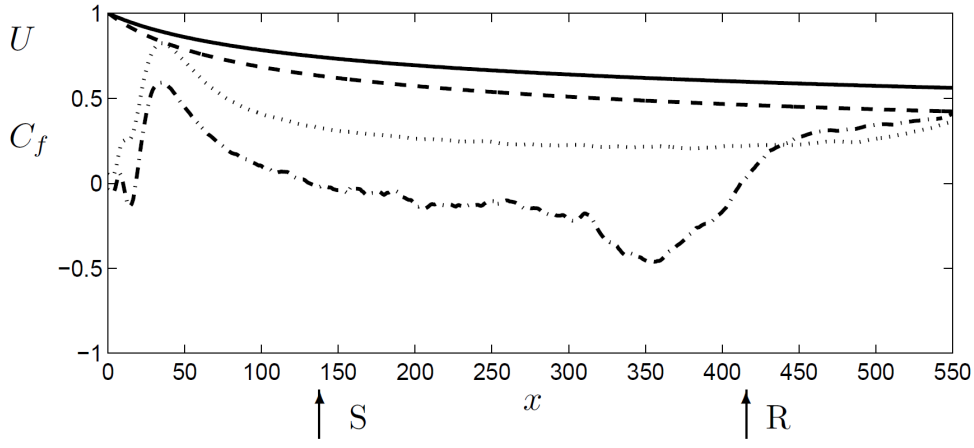


Figure 1. APG1: —  $U$ ;  $\cdots$   $C_f \times 100$ . SEP: --  $U$ ; - · -  $C_f \times 100$ . S and R denote the points of separation and reattachment respectively for SEP.

Table 2. Some parameters of the turbulent boundary layers at different downstream positions.

	APG1	SEP		
	$x = 150$	$x = 300$	$x = 412$	$x = 450$
$U$	0.73	0.51	0.46	0.45
$u_\tau$	0.0287	0.0165	0.0024	0.0166
$u_p$	0.0117	0.0086	0.0074	0.0071

scales used in the near-wall damping is analyzed in section 3.4. In section 3.5 some examples of the performance of the EARSM model are shown, using the data from DNS.

### 3.1. Description of the test cases

The data from the two turbulent boundary layers considered in the present work were taken from a DNS performed by Skote and Henningson (2002).

The freestream velocity ( $U$ ) for the two simulations, APG1 and SEP, are shown in figure 1, together with the skin friction ( $C_f$ ). As seen from the figure, a small change in the freestream velocity has a great impact on the skin friction. In APG1, the boundary layer is subject to a strong APG, but is everywhere attached. In SEP the boundary layer is separated for a large portion of the computational domain.

The simulations start with a laminar boundary layer at the inflow ( $x = 0$ ) which is triggered to transition by a random volume force near the wall. The flow is fully turbulent at  $x = 100$ .

The downstream coordinate  $x$  is scaled with the displacement thickness ( $\delta^*$ ) at the starting position of the simulation ( $x = 0$ ), where the flow is laminar and  $Re_{\delta^*} = 400$ .

Table 2 serves as a comparison of the two cases at the downstream positions investigated in the present work.

### 3.2. APG1

In this section different modelling assumptions are tested by using DNS data from the attached APG boundary layer (APG1). The anisotropies are calculated from equation (14) with  $S_{ij}$  and  $\Omega_{ij}$  computed from DNS data. The resulting anisotropies are then compared with those taken directly from the DNS.

The shear anisotropy  $a_{12}$  is plotted for one streamwise position ( $x = 150$ ) in figure 2. The behaviour is approximately the same at all streamwise positions for APG1. The anisotropy taken

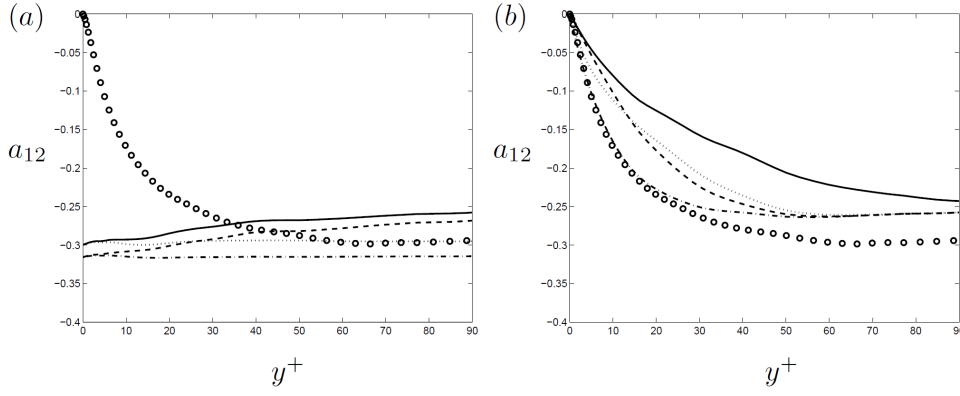


Figure 2. APG1 at  $x = 150$ : (a)  $\circ$  DNS; — non-damped "W&J";  $\cdots$  non-damped "W&J" with  $\beta_4 = 0$ ; - - non-damped "Gir"; --- non-damped "Gir" with  $\beta_4 = 0$ . (b)  $\circ$  DNS. Damped "W&J" with the scaled coordinate in  $f_1$  as —  $y^+$ ; - -  $y^*$ ;  $\cdots$   $y^T$ . --- damped "W&J" with  $y^+$  and  $A^+ = 11$ .

directly from DNS data is shown with circles. The non-damped models "W&J" and "Gir" are shown in figure 2a. Both models overpredict the asymptotic value at large  $y^+$ , which is around -0.3 in the DNS data. The failure to correctly predict the asymptotic value is due to that the basic, undamped, models do not correctly respond to the pressure gradient. The error enters mainly through the non-linear term in equation (14a) and the best result is actually obtained with  $\beta_4 = 0$  for the "W&J" model, as shown in figure 2a with the dotted line. Setting  $\beta_4 = 0$  should, however, not be considered as an alternative for improving the model behaviour since the  $\beta_4$  term results from a formal approximation of the basic Reynolds stress transport model. Moreover, the  $\beta_4$  term gives important contributions for the normal anisotropy components.

Near the wall, damping with  $f_1$  becomes important. The  $a_{12}$  profiles from the damped "W&J" model are shown in figure 2b. The standard van Driest damping, equation (20), with the standard value of  $A^+ = 26$ , does not give the correct near-wall damping (the solid line in figure 2b). Thus, the standard van Driest damping, which gives a good agreement for a ZPG boundary layer, must be improved in order to give reasonable results for an APG flow. The most straight forward correction is to change the value of  $A^+$  in equation (20).

The damped profiles give very different results depending on the value of  $A^+$ . The value of  $A^+ = 11$  was observed to give the best agreement with the DNS data, (the dash-dotted profile in figure 2b), and by setting  $\beta_4 = 0$  almost perfect agreement with DNS was obtained.

There are many relations between  $A^+$  and the ratio  $u_p/u_\tau$  proposed in the literature. Kays (1971) proposed the relation,

$$A^+ = \frac{26}{1 + 30.18 \left( \frac{u_p}{u_\tau} \right)^3}, \quad (23)$$

which gives a value of  $A^+ = 8.6$  for APG1. This value is far from the standard value of 26, but does not agree with the best fitted value of 11 for APG1. In the experimental work of Nagano, Tagawa, and Tsuji (1992) however, the formula (23) gave good predictions. Cebeci (1970) proposed the relation,

$$A^+ = \frac{26}{\sqrt{1 + 11.8 \left( \frac{u_p}{u_\tau} \right)^3}}, \quad (24)$$

which gives a value of  $A^+ = 19.4$  for APG1. This value is closer to 26, but far from the value of 11. Granville (1989) proposed a relation which is similar to equation (24), with a factor of 12.6 instead



of 11.8, which gives very similar values of  $A^+$  as the relation (24).

A list of other relations is included in the work of Granville (1989). However, the above relations were derived from a mixing length hypothesis, which states that the Reynolds shear stress is linked to the velocity gradient through,

$$-\langle u'v' \rangle^+ = (l^+)^2 \left( \frac{du^+}{dy^+} \right)^2, \quad (25)$$

with

$$l^+ = \kappa y^+ f_1 \quad \text{or} \quad l^+ = \kappa y^* f_1, \quad (26)$$

and  $f_1$  as in equation (20). The coordinate  $y^*$  is given in equation (9). The second form of  $l^+$  above (26b) was, among others, used by Granville (1989). However, he let a factor  $\alpha$  reduce the influence of the pressure gradient,

$$y^* = \sqrt{(y^+)^2 + \alpha \left( \frac{u_p}{u_\tau} \right)^3 (y^+)^3} \quad (27)$$

There is some discrepancy regarding the value of  $\alpha$  in the literature. Perry, Bell, and Joubert (1966) proposed a varying  $\alpha$  from 0.65 to 0.9, while Granville (1989) specified 0.9 and McDonald (1969) 0.7. When Skåre and Krogstad (1994) investigated the formula (26b), they had to change the value of  $\kappa$  from 0.41 to 0.78 to fit with experimental data through the logarithmic layer. In the present investigation, the influence of  $\alpha$  and  $\kappa$  will not be considered important, since the goal is not to create a mixing length theory, but to use the best damping function for the EARS model.

In the EARS model, the relation between the Reynolds shear stress and the velocity gradient is more complicated than equation (25), and an analysis is not as straightforward. The damping with  $f_1$  as in equation (20), which was developed from the mixing-length theory, has proved to work well for the EARS model for channel flow and ZPG boundary layer flow. For the APG boundary layer flow however, the damping of both the mixing-length theory, equation (25), and the EARS has to be developed. To further investigate this idea for the EARS model, where no mixing length exists, the viscous scaling of the normal coordinate in  $f_1$  is substituted with the  $y^*$ , defined in section 2.1.

Arguing that  $u_\tau$  no longer is the relevant velocity scale, the scaled normal coordinate  $y^+$  in equation (20) may be changed to  $y^*$ . A different length scale was proposed by Wallin and Johansson (2000), and their scaled normal coordinate  $y^T$ , is defined as,

$$y^T = C_{y1} \sqrt{Re_y} + C_{y2} Re_y^2, \quad (28)$$

where  $Re_y = \sqrt{K}y/\nu$ ,  $C_{y1} = 2.4$  and  $C_{y2} = 0.003$ .

Thus, the damping function  $f_1$  can be expressed as,

$$f_1 = 1 - \exp(-y^*/A^+), \quad (29)$$

or

$$f_1 = 1 - \exp(-y^T/A^+). \quad (30)$$

The formulation of  $f_1$  as in equation (29) was actually used for the mixing length damping by Cebeci and Smith (1968).

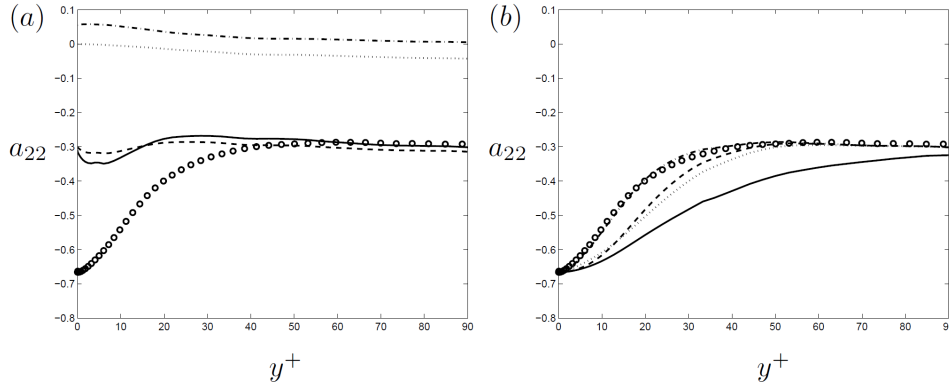


Figure 3. APG1 at  $x = 150$ : (a)  $\circ$  DNS; — non-damped "W&J";  $\cdots$  non-damped "W&J" with  $\beta_4 = 0$ ; - - non-damped "Gir"; --- non-damped "Gir" with  $\beta_4 = 0$ . (b)  $\circ$  DNS. Damped "W&J" with the scaled coordinate in  $f_1$  as —  $y^+$ ; - -  $y^*$ ;  $\cdots$   $y^T$ . --- damped "W&J" with  $y^+$  and  $A^+ = 11$ .

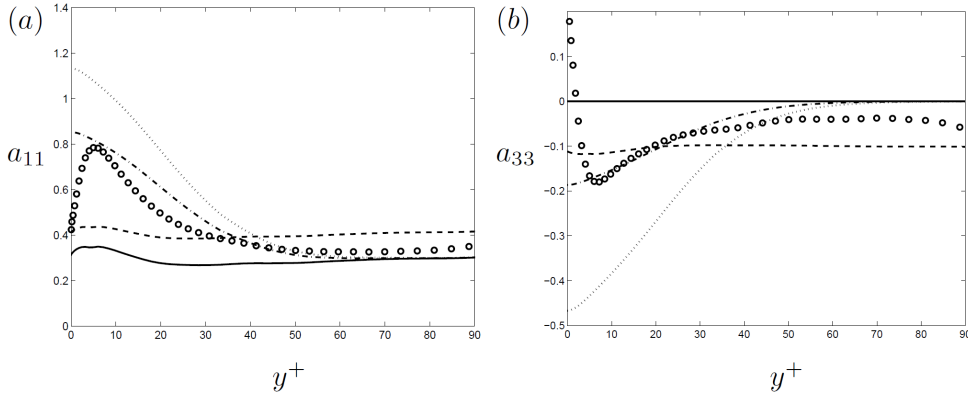


Figure 4. APG1 at  $x = 150$ . (a)  $a_{11}$ . (b)  $a_{33}$ .  $\circ$  DNS; — non-damped "W&J"; - - non-damped "Gir";  $\cdots$  damped "W&J" with the scaled coordinate in  $f_1$  as  $y^T$ ; --- same as the previous profile but with  $B_2=1.52$ .

A third possibility would be to use  $y^p$ . However, to change from  $y^+$  to  $y^p$  cannot give any improvement since they are linearly dependent of each other. Thus, the same  $f_1$  profile can be obtained by using  $y^+$  or  $y^p$  if the constant  $A^+$  is adjusted.

In figure 2b, the "W&J" model damped with  $f_1$  based on the scaled normal coordinates  $y^*$  and  $y^T$  are shown. They work almost equally well and the original value of  $A^+ = 26$  was kept.

Since the dependency of  $A^+$  on the pressure gradient and Reynolds number ( $u_p/u_\tau$ ) seems difficult to describe correctly, the rescaled functions (29) and (30) are good alternatives for achieving proper damping in APG flows.

The good results obtained with  $\beta_4 = 0$  for  $a_{12}$  is not consistent with the results for  $a_{22}$ , shown in figure 3. Here, the  $\beta_4$  coefficient is important to get agreement with DNS data for large values of  $y^+$ . Both the "W&J" and "Gir" models predict the asymptotic value of  $a_{22}$  well. The profiles from the damped "W&J" model are shown in figure 3b. The alternative length scales  $y^*$  and  $y^T$  with  $A^+ = 26$  are also here very similar and give clear improvements compared to the  $y^+$  scaling. The best fit is obtained by using  $y^+$  with  $A^+ = 11$  also in this case.

The anisotropies  $a_{11}$  and  $a_{33}$  are shown in figure 4a and b. For  $a_{11}$  the "W&J" model gives better agreement with DNS data at large  $y^+$  than the "Gir" model. The damped "W&J" model gives profiles with the same trend as for  $a_{12}$  and  $a_{22}$ , i.e. the alternative length scales  $y^*$  and  $y^T$  with  $A^+ = 26$  work equally well as  $y^+$  with  $A^+ = 11$ . Only the  $y^T$  damped profile is shown (dotted line) in figure 4a. For  $a_{33}$  (figure 4b), the non-damped "W&J" model predicts a value of zero. However, the "Gir" model does not give a better prediction even though it is non-zero. The damped "W&J" model results in a profile (dotted line) that gives a poor agreement with DNS data close

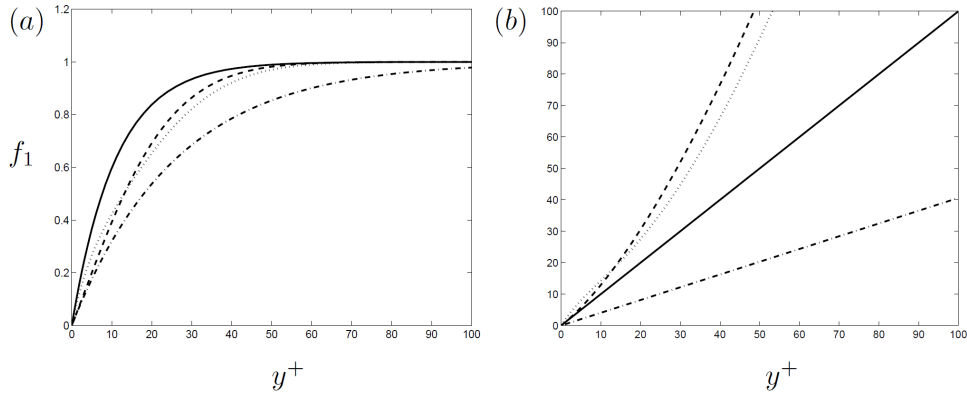


Figure 5. APG1 at  $x = 150$ : (a)  $f_1$  using —  $y^+$  and  $A^+ = 11$ ; - -  $y^*$  and  $A^+ = 26$ ;  $\cdots$   $y^T$  and  $A^+ = 26$ ; -·-  $y^+$  and  $A^+ = 26$ . (b) —  $y^+$ ; - -  $y^*$ ;  $\cdots$   $y^T$ ; -·-  $y^P$ .

to the wall. The wall values of  $a_{11}$  and  $a_{33}$  are controlled by the  $B_2$  coefficient, and by modifying that to 1.52 almost perfect agreement is obtained (see figure 4). The original value  $B_2 = 1.8$  was calibrated from channel flow and the different value obtained for this case indicates that there are a pressure-gradient dependency in  $B_2$ .

The damping functions are shown in figure 5a. The function based on  $y^+$  with the optimal value of  $A^+ = 11$ , and the functions based on  $y^*$  and  $y^T$  reach unity after approximately  $y^+ = 40$ . Thus, the damping has no effect for  $y^+$  over approximately 40. The change from the original shape (with  $y^+$  and  $A^+ = 26$ ) is large. In figure 5b the scaled normal coordinates are shown as a function of  $y^+$ . From figure 5b it is noted that  $y^P$  is proportional to  $y^+$ , which is obvious since both  $u_\tau$  and  $u_p$  are independent on  $y$ .

In conclusion, the change from  $y^+$  to  $y^*$  or  $y^T$ , is recommended in favour of keeping the  $y^+$  scaling where the value of  $A^+$  has to be changed for different APG layers. A specific value has to be obtained for each APG and also for each downstream position if the range of Reynolds numbers is large. The value of  $A^+ = 11$  is only valid for the APG1 case presented here. For a less severe APG, the value of  $A^+$  has to be increased, whereas the scaling with  $y^*$  or  $y^T$  can be kept intact. In the extreme case of  $u_\tau = 0$ , the formulation with  $y^*$  or  $y^T$  is still valid, whereas the  $y^+$  formulation encounters a singularity, no matter what value of  $A^+$  being used. The extreme case of ZPG is the limit where the value of  $A^+$  is 26 in  $y^+$  formulation and the formulation with  $y^*$  is equivalent with the  $y^+$  damping since  $y^* = y^+$  for a ZPG boundary layer.

### 3.3. SEP

From the case with separation (SEP), three positions will be investigated. The positions are taken from the separated region ( $x = 300$ ), at the reattachment point ( $x = 412$ ), and in the recovery region ( $x = 450$ ). The profiles are presented as functions of  $y^+$  at all positions. Observe that the friction velocity is defined from the absolute value of the wall shear stress, so it is everywhere positive.

At  $x = 300$  the boundary layer is separated. At this position the non-linear term in the model expression for  $a_{12}$  does not give the same strong contribution to the distribution of  $a_{12}$  as in the APG1 case (see figure 6a).

The difference between the "W&J" and "Gir" models is suppressed at this position where the boundary layer is separated, as seen from figure 6a.

The near-wall behaviour is entirely different from an attached layer. The non-damped profiles reach up to a positive value of 0.3 at the wall, due to that  $S_{12}$  is negative in a separated case.  $S_{12}$  at  $x = 300$  is shown in figure 9a as the solid line. The two other profiles are the  $S_{12}$  for  $x = 412$  and  $x = 450$ . Both in the APG1 case and in the SEP case in the attached region ( $x = 450$ ), the non-damped profiles reach a value of  $-0.3$  at the wall, because  $S_{12}$  is positive at those positions.

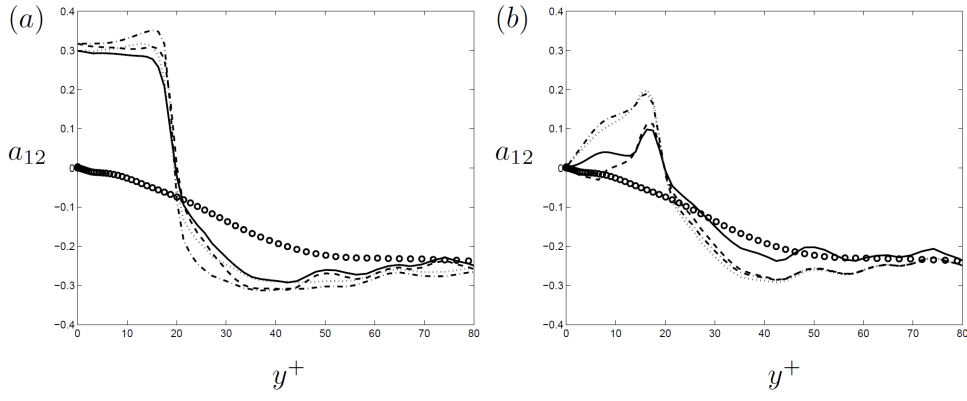


Figure 6. SEP at  $x = 300$ : (a)  $\circ$  DNS; — non-damped "W&J"  $\cdots$  non-damped "W&J" with  $\beta_4 = 0$ ; - - non-damped "Gir"; --- non-damped "Gir" with  $\beta_4 = 0$ . (b)  $\circ$  DNS. Damped "W&J" with the scaled coordinate in  $f_1$  as —  $y^+$ ; - -  $y^*$ ;  $\cdots$   $y^T$ . --- damped "W&J" with  $y^+$  and  $A^+ = 11$ .

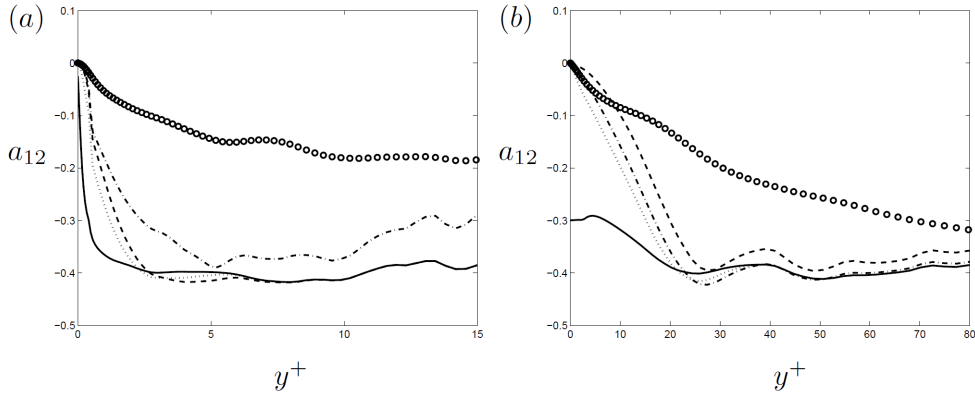


Figure 7. SEP at (a)  $x = 412$ . (b)  $x = 450$ .  $\circ$  DNS; — non-damped "W&J". Damped "W&J" with the scaled coordinate in  $f_1$  as - -  $y^*$ ;  $\cdots$   $y^T$ ; ---  $y^+$ .

The damped "W&J" model at  $x = 300$  is shown in figure 6b. Since the pressure gradient is more severe in this case (SEP), we do not expect the same value of  $A^+$  to give the good agreement as for APG1 (remember that  $A^+$  depends strongly on  $u_p/u_\tau$ ). Actually, the value of  $A^+ = 26$  (solid line) gives better agreement than  $A^+ = 11$  (dash-dotted line) in this case, as seen in figure 6b.

When using  $y^T$  in the expression for  $f_1$ , no much difference from the case of  $y^+$  together with  $A^+ = 11$  can be detected, see figure 6b. The  $y^*$  damping (dashed line in figure 6b) gives a better agreement near the wall. This is due to that  $y^*$  is zero close to the wall where the back-flow occurs, see equation (12).

At  $x = 412$  the boundary layer is at its reattachment point. The DNS data and profiles from the EARSIM are shown in figure 7a. At this position the non-damped profile from the "W&J" model stretches up to zero instead of approaching a constant value at the wall. This is due to that  $S_{12}$  goes to zero at the wall (zero wall shear stress).  $S_{12}$  at  $x = 412$  is shown in figure 9a as the dashed line. Note that the boundary layer is much thinner in the viscous scaling at  $x = 412$  due to the low value of  $u_\tau$  at reattachment.

It is interesting to note in the DNS data that  $a_{12}$  is negative also in the separation bubble where  $S_{12}$  is negative. Hence, the turbulence production as well as an effective eddy viscosity is actually negative, which an algebraic model cannot reproduce. This effect is probably due to transport of the anisotropy in the thin near-wall layer.

At  $x = 450$  the boundary layer is attached, and the near-wall behaviour is the same as for APG1. The value of  $-0.3$  is obtained with the non-damped "W&J" model, shown with the solid line in figure 7b. There is not much difference between the three different versions of the damping function,

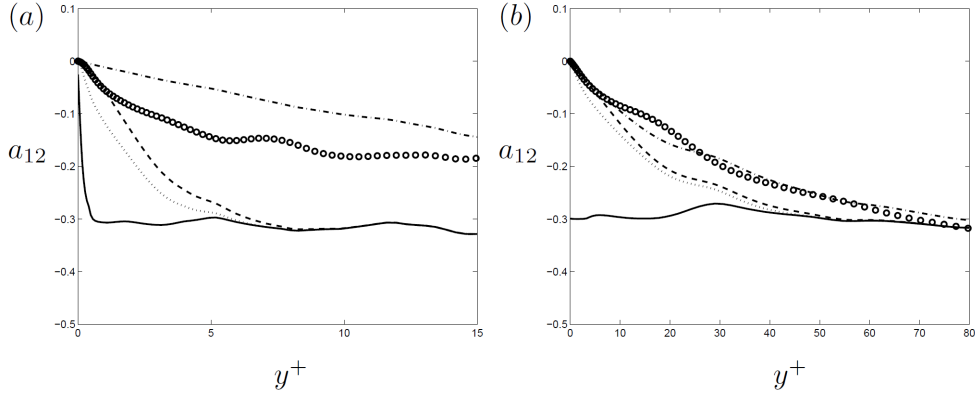


Figure 8.  $a_{12} = f_1 \beta_1 S_{12}$ . SEP at (a)  $x = 412$ . (b)  $x = 450$ .  $\circ$  DNS; — undamped "W&J" ( $f_1 = 1$ ). Damped "W&J" with the scaled coordinate in  $f_1$  as --  $y^*$ ;  $\cdots$   $y^T$ ; -.-  $y^+$ .

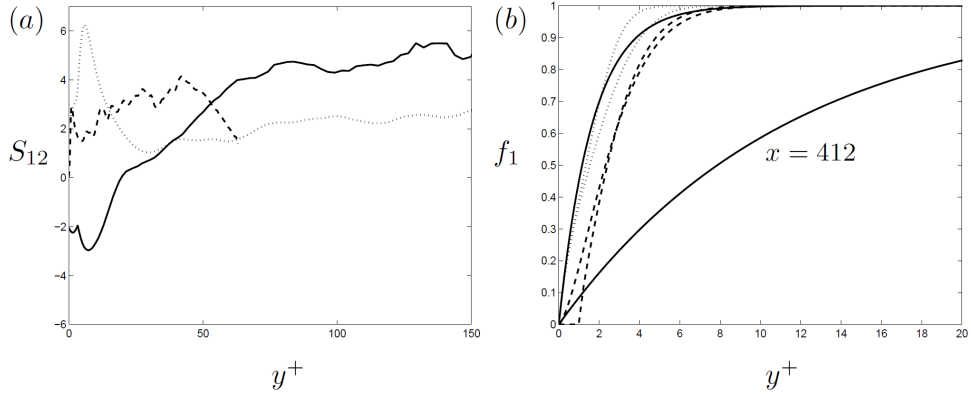


Figure 9. SEP: (a)  $S_{12}$  at —  $x = 300$ ; --  $x = 412$ ;  $\cdots$   $x = 450$ . (b)  $f_1$  at  $x = 412$  and  $x = 300$ , using —  $y^+$ ; --  $y^*$ ;  $\cdots$   $y^T$ .

shown in figure 7b. The value  $A^+ = 26$  was used for the damped model predictions in figures 7a and b. However, the damping is insensitive to the value of  $A^+$  at both positions  $x = 450$  and  $x = 412$ . The damping is insufficient for all versions of  $f_1$ , and the reason is that the non-linear terms have influence in this region.

The general near-wall behaviour is the same for both positions  $x = 450$  and  $x = 412$ , except for the important fact that also the non-damped profile at the wall is zero at  $x = 412$ , due to that the boundary layer is at its reattachment point. Even though the non-damped profiles are 'naturally' damped due to the value of zero at the wall, the damping works just as bad as for the position  $x = 450$ .

Thus, at both positions  $x = 450$  and  $x = 412$  (figures 7a and b), it is observed that the damping does not work very well. However, since the equation (14) is dependent on both the linear and non-linear terms, the effect of the damping is complicated. To isolate the effect of the damping of the linear term, only the first part of the expression for  $a_{12}$  is shown in figure 8a and b. The damping works very well on the linear part, especially for the position where the boundary layer is attached, figure 8b. The damping based on  $y^*$  or  $y^T$  gives as good agreement as  $y^+$ .

The different versions of the function  $f_1$  (20, 29, 30) are shown at two downstream positions in figure 9b. The formulation with  $y^+$  yields very different shapes at the two positions, whereas  $y^*$  and  $y^T$  give profiles close to each other. Note that  $f_1$  based on  $y^*$  is zero up to  $y^+ = 1$  at  $x = 412$ .

The damping functions at  $x = 412$  are shown in figure 10a. The function based on  $y^+$  increases very slowly while the functions based on  $y^*$  and  $y^T$  reach unity after approximately  $y^+ = 8$ . In figure 10b, the scaled normal coordinates are shown as a function of  $y^+$ . The largest difference between the three coordinates are found at this position where reattachment occurs ( $x = 412$ ).

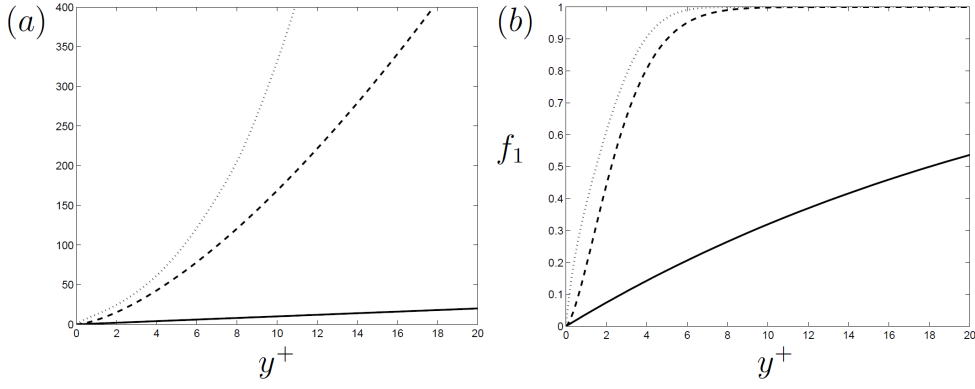


Figure 10. SEP at  $x = 412$ : (a) —  $y^+$ ; --  $y^*$ ; ...  $y^T$ . (b)  $f_1$  using —  $y^+$ ; --  $y^*$ ; ...  $y^T$ .

### 3.4. Similarities between the $y^*$ and $y^T$ scalings

Let us try to analyze why the  $y^*$  and  $y^T$  scalings behave similarly. The  $y^T$  relation is written in terms of  $Re_y$  according to (28). The dominating term, at least for small  $Re_y$ , is the  $\sqrt{Re_y}$  term so essentially  $y^T \sim \sqrt{Re_y}$ . The  $\sqrt{Re_y}$  term is simply motivated by that  $Re_y \sim y^2$  since  $K \sim y^2$  and the wanted behaviour is  $y^T \sim y$  in the very near-wall region (the viscous sub-layer).

In the log region of the boundary layer there is another relation between  $Re_y$  and the  $y^*$  scaling that may be derived from the following. Let us first rewrite  $Re_y$  by using that  $\langle u'v' \rangle = Ka_{12}$  as

$$Re_y \equiv \frac{y\sqrt{K}}{\nu} = y^+ \sqrt{K^+} = \frac{1}{\sqrt{-a_{12}}} y^+ \sqrt{-\langle u'v' \rangle^+} \quad (31)$$

Away from the viscous sub-layer, the viscosity may be neglected and then  $-\langle u'v' \rangle^+ \approx 1 + (u_p/u_\tau)^3 y^+$  (see equation 5). By using the relation (9) the Reynolds number may be related to  $y^*$  as

$$Re_y \approx \frac{1}{\sqrt{-a_{12}}} \sqrt{(y^+)^2 + \left(\frac{u_p}{u_\tau}\right)^3 (y^+)^3} = \frac{y^*}{\sqrt{-a_{12}}} \quad (32)$$

Since  $a_{12}$  is rather constant (and independent of the pressure gradient) away from the wall there is a linear relation  $Re_y \sim y^*$  in the log layer and  $Re_t$  and  $y^*$  could be expected to respond similarly to pressure gradients.

However, the leading order term in the  $y^T$  scaling is proportional to  $\sqrt{Re_y}$  and, thus,  $y^T \sim \sqrt{y^*}$ . The  $\sqrt{Re_y}$  dependency is adopted considering the viscous sub-layer where the assumption of neglected viscosity in (32) is basically wrong. This analysis, thus, only gives a qualitative explanation of the relation between  $y^*$  and  $y^T$  but gives an idea of why the two scalings behave similarly.

### 3.5. Performance of the EARS model

The APG1 boundary layer was computed with a boundary layer solver using different turbulence models. The DNS data at  $x = 150$  were used as inflow condition to the boundary layer computations.

The turbulence models tested are the Wallin & Johansson (2000) EARS model with the wall-damping function based both on  $y^+$  and  $y^T$ , the corresponding EARS model based on the linearized SSG model (Girimaji 1997) with the Wallin & Johansson wall-damping function based on  $y^T$ , the Chien (1982) eddy-viscosity  $K - \varepsilon$  model, and the Hanjalić, Jakirlić, and Hadžić (1995) RST model. All three EARS models are solved together with the Wilcox (1994) low-Reynolds number  $K - \omega$  model.

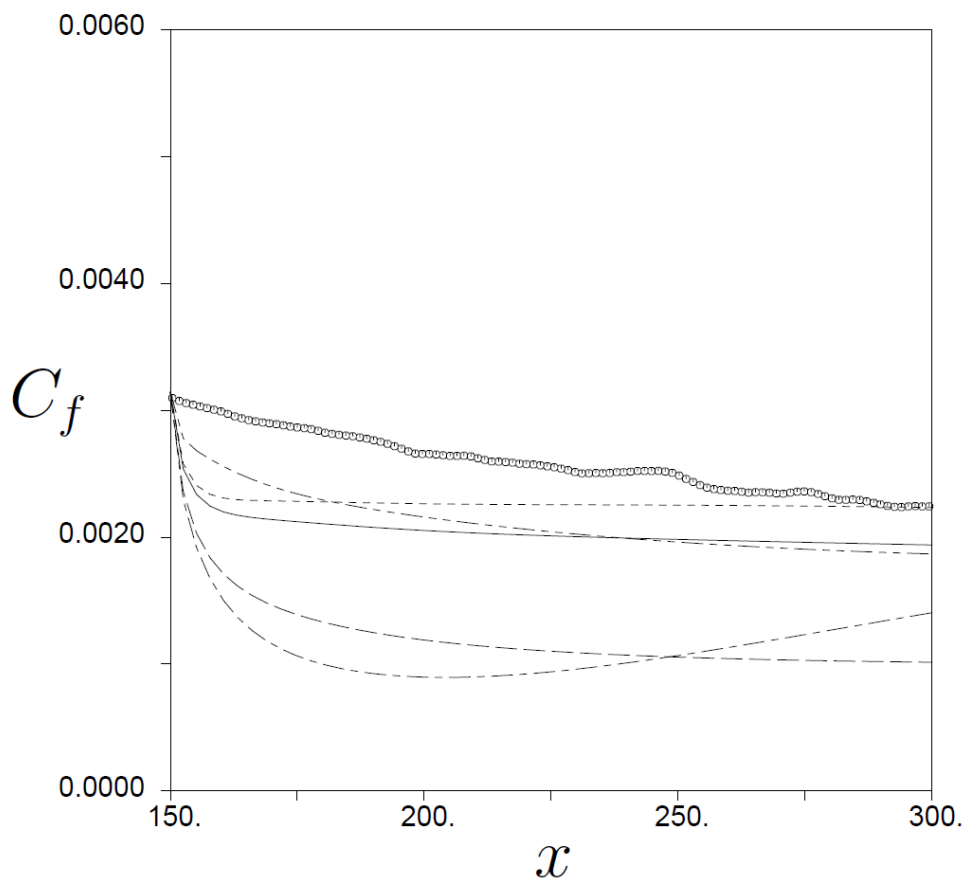


Figure 11. Computed skin friction coefficient  $C_f$  of the flat plate APG1 boundary layer compared to DNS data: — W&J EARSM with  $y^T$  damping; - - W&J EARSM with  $y^+$  damping; - . - Girimaji EARSM with  $y^T$  damping; . . . Chien  $K - \epsilon$ ; - - - Hanjalic RST.

Figure 11 shows the computed skin friction coefficient compared with DNS data. After an initial transient the computed skin friction levels out to some asymptotic behaviour. The transient is caused by inconsistency between the inflow data and the turbulence model. In the computations the coefficient  $\beta \equiv \frac{\delta^*}{\tau_w} \frac{dP}{dx}$  was kept constant which leads to a reduced effect of the transient even though the extent of the transient is rather large since the Reynolds number is relatively low. Computations with a given pressure gradient resulted in a separated flow for the  $y^+$  based models, which will not be reported here.

There are two models that significantly deviates from the other models. These are the Chien  $K - \epsilon$  and the Wallin & Johansson EARSM with the wall-damping function based on  $y^+$ . The wall-damping function in the Chien model is also based on  $y^+$ . The other models do not use wall-damping functions based on  $y^+$  and it is a reasonable assumption that the  $y^+$  scaling is the major cause of the deviations. That is clearly seen if one compares the two computations using the Wallin & Johansson EARSM where the only difference between these two is the wall length scaling ( $y^+$  or  $y^T$ ).

Figure 12 shows the computed velocity profile compared with DNS data. Also here it is observed that the models with  $y^+$  based near-wall damping compares bad with the DNS data while the other models are reasonably accurate. Also here one can notice the difference between the two computations using the Wallin & Johansson EARSM.

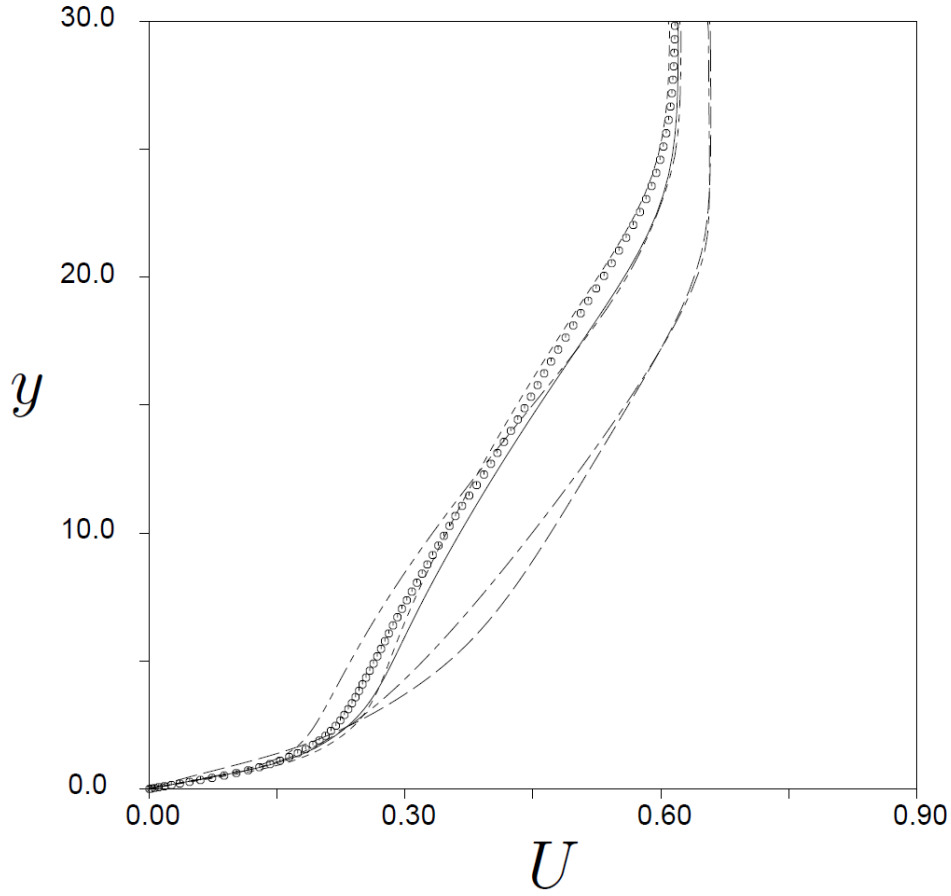


Figure 12. Computed mean velocity profiles at  $x = 350$  for APG1 compared to DNS data.  $\circ$  DNS data; — W&J EARSM with  $y^T$  damping; -- W&J EARSM with  $y^+$  damping; - . - Girimaji EARSM with  $y^T$  damping; - - - Chien  $K - \varepsilon$ ; - - - Hanjalić RST.

#### 4. Conclusion

The viscous sub-layer in the near-wall boundary layer is largely governed by transport and non-equilibrium phenomena, which, in principle, only can be captured by full Reynolds stress models. Eddy-viscosity models as well as algebraic Reynolds stress models must, thus, be modified by more or less empirical near-wall damping functions in order to have the correct near-wall asymptotic behaviour.

Near-wall damping functions based on  $y^+$  become singular in separation or reattachment points and it was shown that the  $y^+$  scaling also behaves badly in attached boundary layers with adverse pressure gradients. An alternative to  $y^+$  was suggested by Wallin & Johansson (2000) and is basically  $y^T \sim \sqrt{Re_y}$  where  $Re_y \equiv \sqrt{K}y/\nu$ . It was found by use of the DNS data (APG1 and SEP) that the  $y^T$  scaling is reasonably similar to the pressure-gradient corrected analytical scaling  $y^*$  even close to separation.

In a general three-dimensional CFD method the formulation in terms of  $y^T$  is more attractive since that can be derived in every grid point by using local field variables and the wall distance. The use of  $y^*$  involves the skin friction of the nearest wall and also the local pressure gradient. Moreover, in general three-dimensional cases the skin friction, pressure gradient, and external flow are not in general aligned which introduces additional complications.

When damping the  $a_{12}$  component of the anisotropy with a van Driest type of wall damping function it was found that the model predictions were much improved by using  $y^T$  or  $y^*$  compared to  $y^+$  but there was still a significant deviation from the DNS data for the APG1 case. It is obvious



that there are other aspects of damping the  $a_{12}$  anisotropy in adverse pressure gradients than the wall distance scaling which could not be resolved within this study.

Comparisons between the Wallin & Johansson EARSM based on a LRR-type of pressure-strain model and the Girimaji EARSM which is based on the linearized SSG show no major differences concerning the near-wall damping. The only significant difference is that the  $a_{33}$  anisotropy component is non-zero for the Girimaji model whereas it is zero for the Wallin & Johansson model away from the viscous sub-layer due to an additional model simplification. However, the deviation from the DNS data is about the same for both models.

## References

- Cebeci, T. 1970. "Behavior of Turbulent Flow Near a Porous Wall with Pressure Gradient." *AIAA J.* 8 (12): 2152–2156.
- Cebeci, T., and A. M. O. Smith. 1968. "A finite-difference solution of the incompressible turbulent boundary-layer equations by an eddy-viscosity concept." 1968 AFOSR-IFP-Stanford Conference. Vol 1.
- Chen, Y.H., and M. Skote. 2015. "Study of lift enhancing mechanisms via comparison of two distinct flapping patterns in the dragonfly *Sympetrum flaveolum*." *Phys. Fluids* 27 (033604) (3).
- Chien, K. Y. 1982. "Predictions of Channel and Boundary-Layer Flows with a Low-Reynolds-Number Turbulence Model." *AIAA J.* 20: 33–38.
- Cuvier, C., J.M. Foucaut, C. Braud, and M. Stanislas. 2014. "Characterisation of a high Reynolds number boundary layer subject to pressure gradient and separation." *Journal of Turbulence* 15 (8): 473–515.
- Girimaji, S. S. 1997. "A Galilean invariant explicit algebraic Reynolds stress model for turbulent curved flows." *Phys. Fluids* 9: 1067–1077. (Also ICASE Report No. 96-38).
- Granville, P. S. 1989. "A Modified Van Driest Formula for the Mixing Length of Turbulent Boundary Layers in Pressure Gradients." *J. Fluids Eng.* 111: 94–97.
- Hanjalić, K., S. Jakirlić, and I. Hadžić. 1995. "Computation of oscillating turbulent flows at transitional  $Re$ -numbers." In *Turbulent Shear Flows 9*, edited by F. Durst, N. Kasagi, and B. E. Launder. 323–342. Springer-Verlag.
- Ibrahim, I.H., and M. Skote. 2012. "Simulations of the linear plasma synthetic jet actuator utilizing a modified Suzen-Huang model." *Phys. Fluids* 24 (113602) (11).
- Kays, W. M. 1971. "Heat transfer to the transpired boundary layer.." ASME Paper No. 71-HT-44.
- Launder, B. E., G. J. Reece, and W. Rodi. 1975. "Progress in the development of a Reynolds-stress turbulence closure." *J. Fluid Mech.* 68: 537 – 566.
- Mårtensson, G., M. Skote, M. Malmqvist, M. Falk, A. Asp, N. Svanvik, and A. Johansson. 2006. "Rapid PCR amplification of DNA utilizing Coriolis effects." *European biophysics journal with biophysics letters* 35 (6): 453–458.
- McDonald, H. 1969. "The effect of pressure gradient on the law of the wall in turbulent flow." *J. Fluid Mech.* 35: 311–336.
- Menter, F. R. 1994. "Two-equation eddy-viscosity turbulence models for engineering application." *AIAA J.* 32: 1598–1605.
- Nagano, Y, M. Tagawa, and T. Tsuji. 1992. "Effects of Adverse Pressure Gradients on Mean Flows and Turbulence Statistics in a Boundary Layer." In *Turbulent Shear Flows 8*, edited by F. Durst, R. Friedrich, B. E. Launder, F. W. Schmitd, U. Schumann, and J. H. Whitelaw. 7–21. Springer-Verlag.
- Perry, A. E., J. B. Bell, and P. N. Joubert. 1966. "Velocity and temperature profiles in adverse pressure gradient turbulent boundary layers." *J. Fluid Mech.* 25: 299–320.
- Skåre, P. E., and P.-Å. Krogstad. 1994. "A turbulent equilibrium boundary layer near separation." *J. Fluid Mech.* 272: 319–348.
- Skote, M. 2014. "Scaling of the velocity profile in strongly drag reduced turbulent flows over an oscillating wall." *Intl J. Heat Fluid Flow* 50: 352–358.
- Skote, M., and D. S. Henningson. 2002. "Direct numerical simulation of a separated turbulent boundary layer." *J. Fluid Mech.* 471: 107–136.
- Skote, M, D. S. Henningson, and R. A. W. M. Henkes. 1998. "Direct numerical simulation of self-similar turbulent boundary layers in adverse pressure gradients." *Flow, Turbulence and Combustion* 60 (1): 47–85.
- Spalart, P. R., and S.R. Allmaras. 1994. "A one-equation turbulence model for aerodynamic flows." *Recherche*

- Aerospatiale* 1: 5–21.
- Speziale, C. G., S. Sarkar, and T. B. Gatski. 1991. “Modelling the pressure–strain correlation of turbulence: an invariant dynamical systems approach..” *J. Fluid Mech.* 227: 245–272.
- Stratford, B. S. 1959. “The prediction of separation of the turbulent boundary Layer.” *J. Fluid Mech.* 5: 1–16.
- Tennekes, H., and J. L. Lumley. 1972. *A First Course in Turbulence*. The MIT Press.
- Townsend, A. A. 1961. “Equilibrium layers and wall turbulence.” *J. Fluid Mech.* 11: 97–120.
- Wallin, S, and A. V. Johansson. 2000. “An explicit algebraic Reynolds stress model for incompressible and compressible turbulent flows..” *J. Fluid Mech.* 403: 89–132.
- Wilcox, D. C. 1993. *Turbulence Modeling for CFD*. DCW Industries, Inc.
- Wilcox, D. C. 1994. “Simulation of Transition with a Two-Equation Turbulence Model..” *AIAA J.* 32: 247–255.